



Cite this: *New J. Chem.*, 2018, 42, 11373

The inherent mechanism of mechanochromism under different stress: electron cloud density distribution, J-type stacking, pore structure and collapse of J-type stacking†

Yunpeng Qi,^a Wenjing Liu,^a Yongtao Wang,^{ib}*^a Lei Ma,^{*b} Yongjiang Yu,^a Yan Zhang^a and Litong Ren^a

Mechanochromic materials usually exhibit different mechanochromic behaviour after being ground, smashed and exposed to ultrasound, however, the inherent mechanisms of these different mechanical stresses have remained elusive until now. In order to unveil the critical factors of mechanochromism, five TPE unit containing difluoroboron beta-diketonate complexes with different alkyl chain lengths were synthesized. The results indicate that the complexes show strong solid state fluorescence emission, remarkable AIE properties and multicolor switching. However, the complexes exhibited irregular mechanochromic behavior upon an increase in the alkyl chain length. Upon grinding, the complexes exhibited red-shifted solid state fluorescence emission, and the degree of the red-shift can be mainly attributed to the initial crystalline emission, which depends on the J-type molecular stacking and electron cloud density distribution. In contrast to what was observed after grinding, ultrasonic treatment and smashing led to a blue-shift in the solid state fluorescence emission, and furthermore, with the former being observed to have a better mechanochromic effect than the latter. Based on detailed crystal analysis, the complexes were found to have a similar J-type stacking but different pore structure or head-to-head stacking, which leads to obvious wavelength shift for **TPEDKBF₂OMe**, **TPEDKBF₂OBu** and **TPEDKBF₂OHe** before/after smashing. For **TPEDKBF₂Ohe**, the stacking of the flexible long alkyl chains is prone to being destroyed and keep head-to-head J-type stacking from great change, preventing an obvious hypochromic shift in the fluorescence emission. For the first time, the inherent mechanism of mechanochromism can be attributed to the collapse of J-type stacking under ultrasonic treatment and smashing. In addition, the solid-state fluorescence emission properties and detailed crystal analysis also show that hydrophobic interactions and the nonpolar environment of the long alkyl chain can effectively enhance the solid-state fluorescence emission and insertion of nonpolar small molecules.

Received 21st November 2017,
Accepted 25th May 2018

DOI: 10.1039/c7nj04543c

rsc.li/njc

Introduction

Conventional organic boron complexes (boron-dipyromethenes, or BODIPYs for short) show good thermal and chemical stability, narrow absorption and emission spectra, high molar absorption

coefficients and fluorescence quantum yields in solution. However, the solid-state fluorescence of BODIPYs is prone to loss or quenching due to intense intermolecular π - π stacking interactions, which limit their application in organic light emitting devices,¹ optical storage,² pressure sensors,³ light conversion agents,⁴ and so on. To avoid a deterioration in the stacking interactions, the application of aggregation induced emission (AIE) effects in many organic boron complexes have been reported.^{5–11} In addition to the enhanced solid-state fluorescence emission, these complexes also exhibit extraordinary stimuli-responsive properties under some external stimuli, such as scraping, rubbing, grinding, heating, compressing, exposure to ultrasound, *etc.* For example, some β -iminoenolate boron complexes bearing non-planar phenothiazine and phenothiazine-*S,S*-dioxide components were found to exhibit multicolor switching in different solid states.¹² Phenothiazine derivatives

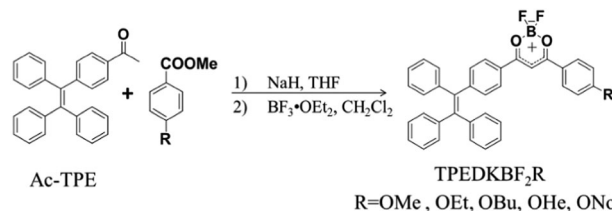
^a School of Chemistry and Chemical Engineering/Key Laboratory for Green Processing of Chemical Engineering of Xinjiang Bingtuan, Shihezi University, Shihezi, 832003, Xinjiang, P. R. China. E-mail: wyt_shzu@163.com; Fax: +86 993 2057270; Tel: +86 993 2057277

^b Tianjin International Center of Nanoparticles and Nanosystem, Tianjin University, Tianjin, 300072, P. R. China. E-mail: maleixinjiang@gmail.com

† Electronic supplementary information (ESI) available: ¹H and ¹³C NMR spectra, mass spectra, single crystal data and other data for the compounds **2a–2e**. CCDC 1558337 (**TPEDKBF₂OMe**), 1832405 (**TPEDKBF₂OEt**), 1832236 (**TPEDKBF₂OBu**), 1832237 (**TPEDKBF₂OHe**) and 1558346 (**TPEDKBF₂ONo**). For ESI and crystallographic data in CIF or other electronic format see DOI: 10.1039/c7nj04543c

with B–N linkages have been reported to have large Stokes shifts, AIE and mechanochromic properties.¹³ Piezochromic boron complexes have been constructed, with a 2-(2'-pyridyl)imidazole functionalized with a triphenylamine unit.¹⁴ Compared with the abovementioned boron complex, a difluoroboron β -diketonate complex has attracted more extensive attention due to its simple synthesis. Yang *et al.*¹⁵ reported a β -diketonate boron complex containing two symmetric carbazole units, showing dual-state fluorescence emission, stimuli-responsive fluorescence and optical waveguide properties. Šket *et al.*¹⁶ prepared a BF_2 complex with polymorphism-dependent fluorescence and mechanochromic properties. Zhang *et al.*¹⁷ also reported several boron-containing compounds that exhibit multicolor switching. Fraser *et al.*¹⁸ constructed mechanochromic difluoroboron β -diketonate complexes by the α position substitution of the dioxaborine ring, subsequently causing a twisted molecular conformation. In our previous work, the tetraphenylethylene (TPE)^{5,19} unit was successfully introduced into difluoroboron beta-diketonate complexes, and some of these were shown to exhibit near 100% solid-state fluorescence quantum efficiency, polymorphism-dependent fluorescence, high contrast mechanochromism and multi-state emission properties. These properties make TPE with a propeller-like conformation an ideal construction unit for synthesizing high performance organic boron complexes. Taking advantage of this change in the fluorescence emission intensity or shifting, high-contrast mechanochromic and multicolour switching organic boron complexes have become attractive for use in industrial applications, such as in anti-counterfeiting,²⁰ memory chips,^{21–24} and biosensors,^{25–27} and in fundamental research.

With much mechanochromic materials being discovered, detailed recent research has revealed that the inherent mechanism of mechanochromism can be mainly attributed to crystal to amorphous, crystal to crystal and amorphous to crystal transitions, isomerization, excimer formation, host–guest interactions, and intramolecular charge transfer.^{28–30} More importantly, the inherent mechanism suggests that just the simple tuning of the intermolecular stacking and arrangement will open up an effective avenue towards obtaining mechanochromic and multicolour switching materials. Thus, researchers have designed and synthesized luminogens with different halogen atoms,^{31,32} heteroatoms,³³ alkyl or alkoxy chains,^{34–42} cyanogens and amino groups.^{43,44} By triggering intermolecular weak interactions and inducing a different molecular stacking and arrangement, as well as gently modifying the molecular skeleton systematically, the relationship between the geometric structure and photophysical properties of the mechanochromic and multicolour switching materials were investigated. Besides this, experimental evidence suggests that few single luminogens exhibit multicolor switching and morphology dependent emission when we change the aggregate morphologies through exerting different forms of stresses to the system, conducting surfactant-assisted self-assembly and changing the crystallization conditions.^{45–47} However, intermolecular weak interactions, and molecular stacking and arrangements are difficult to predict in advance, thus, the mechanochromic properties of luminogens



Scheme 1 The synthetic routes for **TPEDKBF₂OMe**, **TPEDKBF₂OEt**, **TPEDKBF₂OBu**, **TPEDKBF₂OHe** and **PEDKBF₂ONo**.

are still difficult to understand and need in-depth study. In addition, most luminogens usually exhibit red-shifted fluorescence emission after grinding, while the effects of smashing and exposure to ultrasound usually lead to blue-shifted fluorescence emission. Despite some inherent mechanisms involving grinding, smashing and exposure to ultrasound having been elaborated, the irregular grinding effects of alkyl chain dependent luminogens still lacks detailed discussion, and the investigation of grinding effects remains rare based on similar J-type stacking. More importantly, the inherent mechanisms of smashing and exposure to ultrasound have remained elusive until now.

To further explore the influence of the alkyl length, grinding, stresses and ultrasonic effects on the solid-state fluorescence and mechanochromic behaviour of luminogens, a systematic study of five TPE unit containing difluoroboron beta-diketonate complexes have been conducted (Scheme 1). We found that the propeller-like molecular configuration of TPE can effectively enhance the solid-state fluorescence emission by preventing intermolecular π – π stacking, moreover, the twisted shape is also a key factor in promoting intermolecular loose stacking, and therefore strengthening the mechanochromism. Since the dioxaborine ring and 1,3-disubstituted benzenes generally tend to form more planar configuration than the TPE unit, and the alkyl chains have a rather smaller steric hindrance, it is easy for these complexes to adopt head-to-head intermolecular stacking due to the asymmetric molecular conformation. Similar intermolecular stacking and intermolecular weak interactions are advantageous for us to acquire a greater depth of understanding on the relationship between intermolecular stacking and solid-state fluorescence or mechanochromism. In particular, based on detailed crystal analysis, the unusual and unreported inherent mechanisms of ultrasonic treatment and smashing effects are revealed in this paper.

Results and discussion

Photophysical properties in solutions

The UV-vis absorption and fluorescence emission spectra of **TPEDKBF₂OMe**, **TPEDKBF₂OEt**, **TPEDKBF₂OBu**, **TPEDKBF₂OHe** and **TPEDKBF₂ONo** in different solvents are shown in Fig. S1 (ESI[†]), and clearly show that all of the complexes have two prominent absorption bands, located at *ca.* 300 nm and 420 nm, in different polarity solvents. The weak absorption band that appears at *ca.* 300 nm can be attributed to the π – π^* transitions of the conjugated aromatic rings, and exhibits a red-shift in the

absorption upon an increase in the polarity of the solvent. The maximum absorption peak at *ca.* 420 nm originates from intramolecular charge transfer (ICT) due to the specific electron-donating properties of the TPE moiety and the characteristic electron-accepting properties of the difluoroboron β -diketonate moiety. This can be unambiguously confirmed from the strong solvent-polarity dependent fluorescence emission spectra. On the other hand, we also noticed that the widths of the half peaks of the fluorescence emission spectra in different solvents were rather narrow, which indicates that these complexes have very good color purity. Besides this, all of the complexes show almost identical photophysical behaviour and there is no indication of any alkyl chain length dependence in solution. This is consistent with the common understanding that the photophysical properties of conjugated organic molecules in solution are hardly affected by alkyl chain length, which has been reported in recent literature.

AIE properties

According to the restriction of the intramolecular rotation mechanism, the twisted conformation of the molecular structure could trigger AIE properties. To determine the AIE properties of the complexes, we used a standard method to investigate the fluorescence emission spectra of the complexes in THF/water solutions with different THF concentrations. All of the **TPEDKBF₂**-derivatives exhibit AIE activity weak fluorescence in THF solution that can be largely enhanced in THF/water solvent (Fig. 1 and Fig. S2, ESI[†]). Taking **TPEDKBF₂OMe** as an example, as shown in Fig. 1, when **TPEDKBF₂OMe** was dissolved in THF, the pure THF solution only emitted a faint green light, which could be attributed to the free rotation of the phenyl rings effectively absorbing the energy of the excitons *via* nonradiative relaxation channels. The fluorescence spectra showed mild changes upon an increase in the water content from 0 to 70%, the reason being that the **TPEDKBF₂OMe** molecules are fully dissolved in the mixtures. However, a dramatic fluorescence

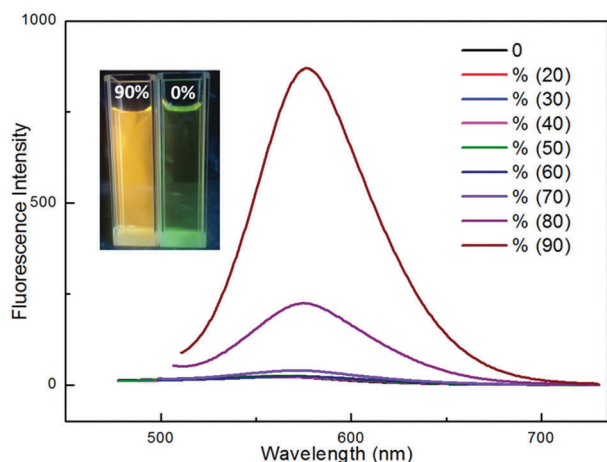


Fig. 1 Fluorescence spectra of **TPEDKBF₂OMe** in THF and THF/water mixtures. Luminogen concentration: 1×10^{-5} mol L⁻¹; excitation wavelength: 420 nm. Inset: Solution of **2a** in THF ($f_w = 0\%$) and its suspension in a THF/water mixture with $f_w = 90\%$; photographs taken under UV illumination.

enhancement behaviour was observed when the water volume fraction (f_w) was increased to 80%, an enhancement that reached a maximum value at about $f_w = 90\%$. The AIE feature was then prominent, with an approximate 40-fold increase observed in the fluorescence intensity. The enhancement of the fluorescence was related to the formation of aggregates, which prevent intramolecular rotation, therefore effectively enhancing the fluorescence. The inset in Fig. 1 shows images of the fluorescence changes in different water containing solvents, which were taken under 365 nm UV illumination.

Solid-state fluorescence and mechanochromic behavior

When yellow crystals of **TPEDKBF₂OMe** (MeOC) were smashed with a stainless steel spoon, the fluorescence emission color of the sample largely underwent changes (Fig. 2). With these changes, the fluorescence intensity of the sample was also enhanced. Thus, MeOC shows mechanofluorochromism (MFC) induced by isotropic pressure. As shown in Fig. 3 and Table 1, the maximum emission band of the smashed sample is centered at 545 nm, and is shifted by about 22 nm after smashing (MeOC crystal has a peak positioned at 567 nm). This indicates that the crystal surface greatly affects the molecular arrangement and packing mode. The powder X-ray diffraction (PXRD) patterns of the crystals before and after smashing were recorded with the aim of figuring out the reasons behind the solid fluorescence hypsochromic effects driven by isotropic pressure. As shown in Fig. 3F, the MeOC crystals show intense and sharp diffraction peaks. After being smashed, the original main peaks are still retained and some new peaks have appeared, and at the same time, some of the pristine peaks were enhanced. This indicates that the molecular perturbations only occurred on the surface, while the molecular arrangements of the main body remain unchanged. Zhang *et al.*⁴⁶ defined the mechanochromic phenomenon as a “disaggregation” process. As for the opposite process of aggregation, this usually gives rise to red-shifted and weakened emission, and disaggregation consequentially leads to blue-shifts and an enhancement in the fluorescence intensity. Meanwhile, the data on the solid fluorescence quantum yield

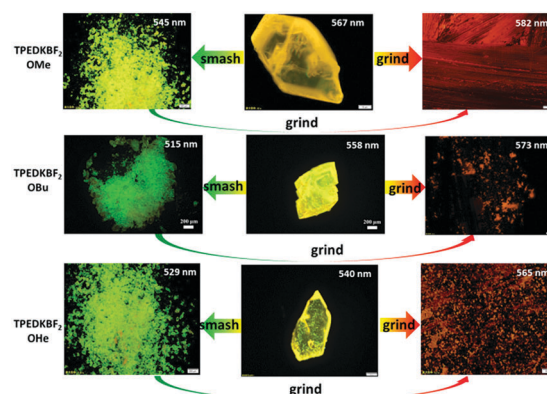


Fig. 2 Photographs of crystals of **TPEDKBF₂OMe**, **TPEDKBF₂OBu** and **TPEDKBF₂OHe** that have been exposed to different stresses (smashing and grinding). The images were obtained using an Olympus BX51 fluorescence microscope.

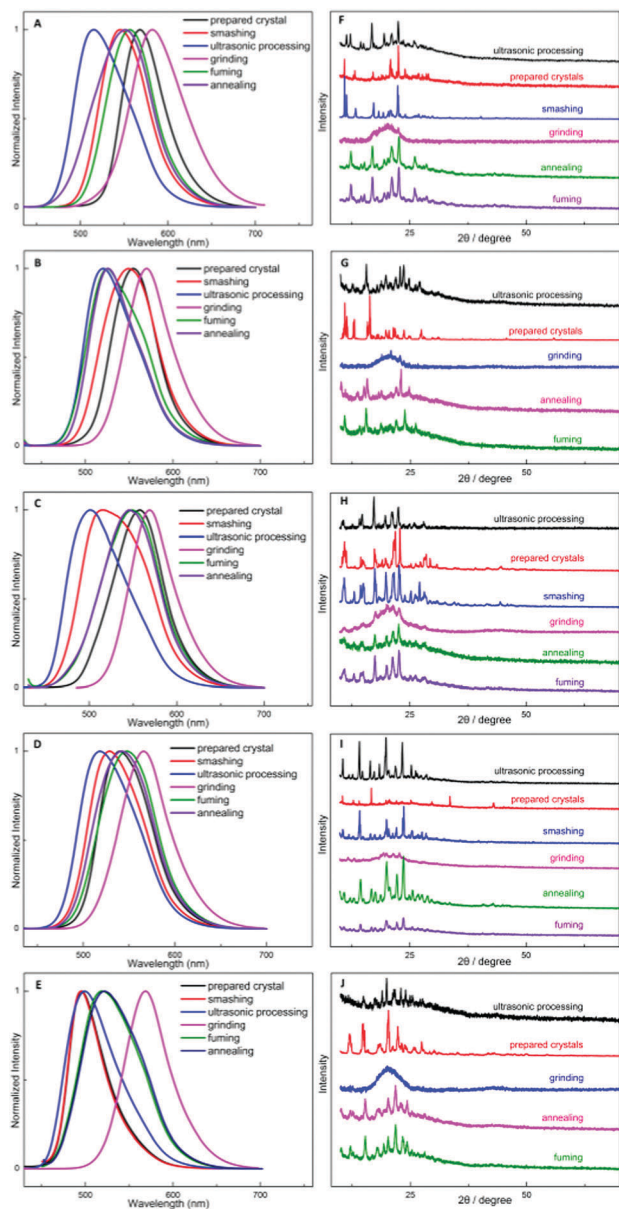


Fig. 3 Fluorescence emission spectra of TPEDKBF₂OMe (A), TPEDKBF₂OEt (B), TPEDKBF₂OBu (C), TPEDKBF₂OHe (D) and TPEDKBF₂ONo (E) in different solid states, and PXRD patterns of TPEDKBF₂OMe (F), TPEDKBF₂OEt (G), TPEDKBF₂OBu (H), TPEDKBF₂OHe (I) and TPEDKBF₂ONo (J) in various states.

also supports this tentative explanation. The quantum yield of the fragmented crystals (0.758) is improved compared with those of the pristine block crystals (0.665), however, the explanation for this is unknown.

To gain more insight into the effects of smashing, we carried out thermal experiments. When the smashed sample was exposed to air at room temperature for two months, the fluorescence emission spectrum remained unchanged. The emission spectrum also remained unchanged after annealing at a temperature of 200 °C. The thermal properties of the smashed sample were evaluated by differential scanning calorimetric analyses, as shown in Fig. 4, and it was found that there were no observed differences the smashed crystals and the

prepared crystals. The same behaviour was observed for the TPEDKBF₂OBu and TPEDKBF₂OHe materials.

We have previously reported that TPE containing difluoroboron β-diketonate complexes show prominent mechanochromism.^{5,19} In this work, the mechanochromic properties of these difluoroboron β-diketonate complexes with different alkyl length were investigated in detail. The fluorescence images of the five compounds in different states are shown in Fig. 5, the emission spectra are displayed in Fig. 3, and the spectroscopic data are summarized in Table 1. The results show that all of the TPEDKBF₂O-derivatives display a fluorescence color change. The emissions of the ground materials are orange, however, this color can be changed to green by simple thermal annealing or solvent-fuming (being exposed to CH₂Cl₂ vapor at room temperature). This process is highly reproducible, indicating typical reversible MFC activity. On the one hand, for the ground powders and pristine solids that have been treated by employing ultrasound in hexane for 30 min, the emission wavelength of the as-prepared samples are all blue-shifted (as shown in Fig. 3). On the other hand, all of the TPEDKBF₂O-derivatives exhibit remarkable grinding-induced peak shifts ($\Delta\lambda_{ML} = \lambda_{ground} - \lambda_{pristine}$), that vary from TPEDKBF₂OMe to TPEDKBF₂ONo (48–72 nm) and show some irregularity. That is, all of the TPEDKBF₂O-derivatives are obviously alkyl chain length-dependent, but do not show any universally direct relationship between the fluorescence emission colour and alkyl chain length. Besides this, regarding the TPEDKBF₂O-derivatives, we observed that for all five of the different samples after ultrasonic treatment in hexane, their crystals have been changed from one form into another. The PXRD patterns of the samples are shown in Fig. 3. The results show that the diffraction signals and fluorescence emission peaks of the ultrasound exposed and the smashed sample are close. These data indicate that the inherent mechanism of smashing and ultrasonic effects may be similar.

In order to gain more insight into the mechanochromic behavior of these different length of alkyl chain containing TPEDKBF₂O-derivatives, we carried out powder X-ray diffraction (PXRD) and differential scanning calorimetry (DSC) experiments on them in different solid states. As shown in Fig. 3, the X-ray diffraction patterns of the pristine solids of all of the TPEDKBF₂O-derivatives show sharp and intense reflections, indicating well-ordered microcrystalline structures. In contrast, the diffractograms of the ground solids display broad and featureless reflections, implying that the structures have changed from a crystalline to amorphous state. In addition, the main diffractive peaks that disappeared reappeared after fuming or annealing treatments, consistent with the reformation of the pristine sample, indicating that the mechanochromic behaviour is reversible. The formation of an amorphous structure after grinding was also confirmed from DSC experiments. As shown in Fig. 4, no exothermic peaks could be detected before the melt transition (T_m , 258 °C), but an endothermic peak appeared at 153 °C in pristine samples of TPEDKBF₂OMe, which we suspect corresponds to a solvent molecule of methanol being thrust into the crystal unit cell. This assumption can be backed up by the experimental results, where a methanol molecule

Table 1 Peak emission wavelengths (λ , in nm), fluorescent lifetime (τ , in μ s) and quantum yields of five compounds in different solid states

	TPEDKBF ₂ OMe	TPEDKBF ₂ OEt	TPEDKBF ₂ OBu	TPEDKBF ₂ OHe	TPEDKBF ₂ ONo
λ_u	515	518	501	517	499
λ_c	567	546	558	540	494
λ_s	545	544	515	529	496
λ_g	582	570	573	565	567
λ_f	556	525	547	546	518
λ_a	550	524	545	540	517
$\Delta\lambda_1$	22	2	43	11	2
$\Delta\lambda_2$	15	24	15	25	73
$\Delta\lambda_3$	67	52	72	48	68
Φ_c	0.665	0.603	0.622	0.666	0.983
Φ_g	0.728	0.422	0.622	0.800	0.601
Φ_s	0.927	0.944	0.763	0.830	0.789
Φ_u	0.905	0.479	0.807	0.881	0.814
τ_c	3.578	29.012	2.931	7.851	0.016
τ_g	4.972	3.927	4.984	9.901	6.584

$\Delta\lambda_1$: crystals were smashed, $\Delta\lambda_2$: crystals were ground, $\Delta\lambda_3$: pristine powder after ultrasonic treatment is ground. u represents ultrasonic. c represents crystals. s represents smashed. g represents ground. f represents fumed. a represents annealed.

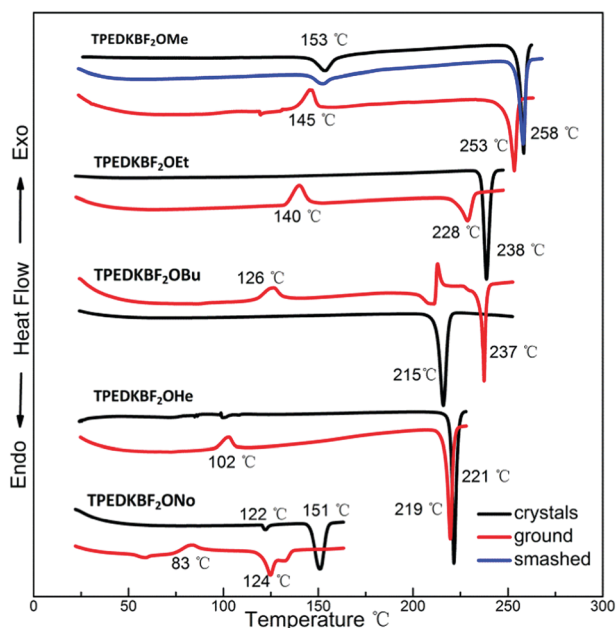


Fig. 4 DSC curves (first heating cycle) of TPEDKBF₂OMe, TPEDKBF₂OEt, TPEDKBF₂OBu, TPEDKBF₂OHe and TPEDKBF₂ONo as crystals after being ground and smashed.

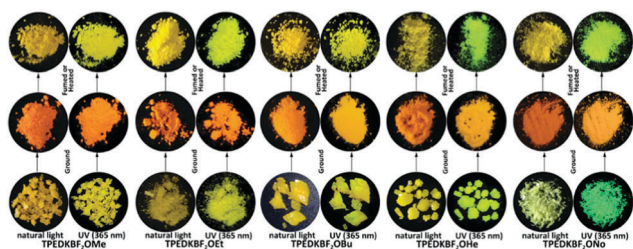


Fig. 5 Photographic images of TPEDKBF₂OMe, TPEDKBF₂OEt, TPEDKBF₂OBu, TPEDKBF₂OHe and TPEDKBF₂ONo, respectively. Obviously, the QY of TPEDKBF₂ONo is much larger compared to those of the other complexes. Meanwhile, all of the complexes, except for TPEDKBF₂ONo, have very close proximity QY values, despite their different J stacking.

was actually found in the crystal unit cell as described above. However, the ground sample shows one clear cold-crystallization

transition (T_c) before T_m , which corresponds to the transition from the amorphous to crystalline state. The thermal behaviour is consistent with the phenomenon observed in the thermal annealing experiments. In addition, these findings suggest that the transformation between the crystalline and amorphous states is the key factor behind the reversible mechanochromism. No other thermal transition peaks were found in the DSC curves for the pristine samples of TPEDKBF₂OEt, TPEDKBF₂OBu and TPEDKBF₂OHe, except for the T_m peaks and similar to TPEDKBF₂OMe, an endothermic peak was found before melting in pristine samples of TPEDKBF₂ONo, and this peak also corresponds to a hexane molecule transferring to the crystal unit cell, because two hexane molecules embed in one unit cell (as shown in Fig. 8). All of the ground samples exhibit a clear cold-crystallization transition (T_c) before T_m . It is worth noting that with an increase in the alkyl chain length, the response temperature of annealing become lower and lower, meanwhile, the T_m also showed a trend of lowering upon an increase in the alkyl chain length. This indicates that the increase in the alkyl chain length could improve the flexibility of the TPEDKBF₂O-derivatives. It is an effective switch that controls the thermal stimulus-response temperature just through introducing different alkyl chains with various lengths.

We also investigated the relationship in those materials between the (crystal state and smashing, grinding, and ultrasonic treatment) fluorescence efficiencies of the solids and their alkyl chain lengths. The data obtained are presented in detail in Table 1. The results indicate that the solid state fluorescence efficiencies (QY) relate to the alkyl chain lengths, but show some irregularity. The fluorescence quantum yields were found to be 0.665, 0.603, 0.622, 0.666 and 0.983 for prepared crystals of TPEDKBF₂OMe, TPEDKBF₂OEt, TPEDKBF₂OBu, TPEDKBF₂OHe and TPEDKBF₂ONo, respectively. Obviously, the QY of TPEDKBF₂ONo is much larger compared to those of the other complexes. Meanwhile, all of the complexes, except for TPEDKBF₂ONo, have very close proximity QY values, despite their different J stacking. Accordingly, it can be inferred that the polarity of hexane and long alkyl chain in the crystal of TPEDKBF₂ONo plays an

important role in the value of the QY. The QYs changed in turn to 0.728, 0.422, 0.622, 0.800 and 0.601 after the samples were ground. Those of **TPEDKBF₂OMe** and **TPEDKBF₂OHe** increased, and those of **TPEDKBF₂OEt** and **TPEDKBF₂ONo** decreased, with no change observed for **TPEDKBF₂OBu**. Based on the PXRD patterns of the complexes in various states (Fig. 3), the irregular changes in the QYs are mainly derived from the regular to irregular molecular stacking. Consistent with the reported literature,⁴⁶ the QYs of the complexes other than **TPEDKBF₂ONo** increased obviously after smashing treatment, which can be interpreted as a process of “disaggregation” at the surface, while the abnormal QY of **TPEDKBF₂ONo** may be due to the solvent effects of hexane. The pore-dependent effect of ultrasonic treatment on the QYs was investigated. **TPEDKBF₂OMe** containing bigger pore structures displayed a significantly enhanced QY, and the collapse of the big pores was beneficial for suppressing the vibration and rotation of the bonds, while the deterioration in the stacking played a major role for **TPEDKBF₂OEt** and **TPEDKBF₂ONo**.

Theoretical calculations and detailed single crystal analysis

To uncover the connection between the irregular dependence upon the alkyl chain length, the smashing, grinding, ultrasonic effects and the solid-state fluorescence and mechanochromic behaviour, theoretical calculations and detailed single crystal analyses were conducted. The density functional theory (DFT) calculations on the complexes **TPEDKBF₂OMe**, **TPEDKBF₂OEt**, **TPEDKBF₂OBu**, **TPEDKBF₂OHe** and **TPEDKBF₂ONo** were conducted using the Gaussian 09W program package, employing the DFT/B3LYP/6-31G basis set. The frontier orbital plots of the HOMO and LUMO are shown in Fig. 6. From the figure, we can see that the HOMO is mainly located on the TPE moiety (electron donor)

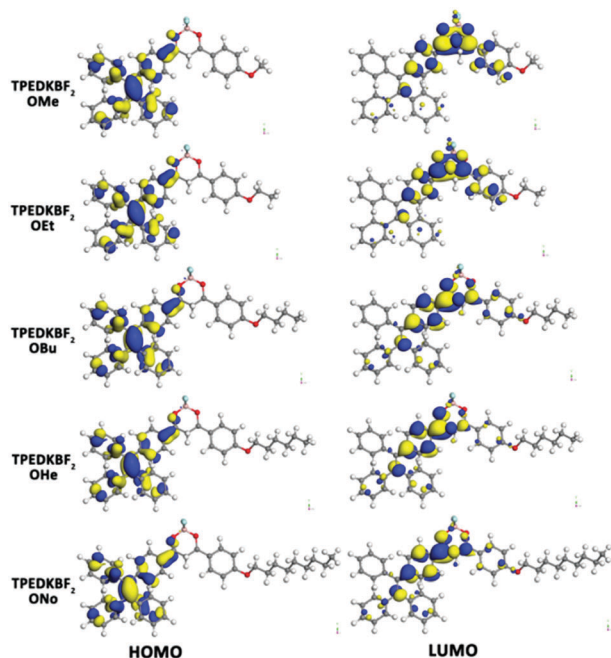


Fig. 6 The frontier orbital plots of the HOMO and LUMO of molecular **TPEDKBF₂OMe**, **TPEDKBF₂OEt**, **TPEDKBF₂OBu**, **TPEDKBF₂OHe** and **TPEDKBF₂ONo**.

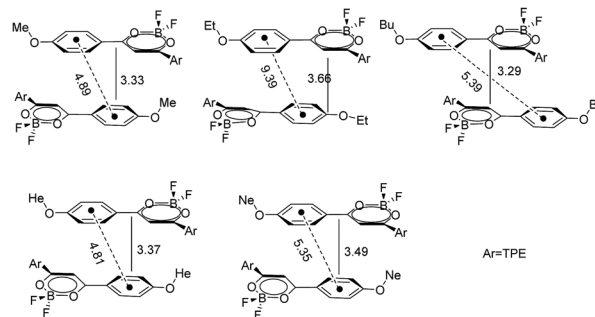


Fig. 7 Head-to-head stacking diagram of the dye molecules in the single crystals (the dotted lines represent the distance between the benzene centers, the solid lines represent the distance between the benzene planes).

and the LUMO is mainly distributed on the acceptor of the β -diketone boron unit in all five of the complexes. Meanwhile, the plot also shows that the LUMOs gradually move to the TPE unit upon an increase in the alkyl chain length. Therefore, intramolecular charge transfer and increased optical energy gaps occur in the D–A type β -diketone boron complexes, with the latter leading to a blue-shift in the fluorescence emission wavelength, which is consistent with the experimental results, in addition **TPEDKBF₂OBu** (Table S1, ESI[†]), was found to have an abnormal red-shift in its fluorescence emission wavelength due to different J stacking (Fig. 8).

To further explore the inherent mechanism of alkyl chain length, stresses and ultrasonic dependent solid state fluorescence and mechanochromism, crystals of the complexes were grown by the slow evaporation of solution. As shown in Fig. 7, 8 and Fig. S3–S7 (ESI[†]), all of the synthetic molecules adopt a head-to-head stacking mode and twisted molecular conformation, in addition, no strong π – π interactions are observed due to the large distances between neighboring molecules in the crystals. Meanwhile, similar intermolecular hydrogen bonds and weak interaction contacts, including C(Ar)–H \cdots F, C(Ar)–H \cdots B, C(Ar)–H \cdots B, were formed in the single crystal that rigidify the rotatable rings to allow them to fit in the crystalline lattice. However, different arrangements and an overlap of the head-to-head stacking led to a larger pore structure in **TPEDKBF₂OMe** compared with that in the other complexes. Apparently, the existence of a large pore structure is advantageous for destroying head-to-head J-type stacking of the molecular surface under isotropic pressure, and thus, **TPEDKBF₂OMe** displays a sharper blue-shift than **TPEDKBF₂OEt** and **TPEDKBF₂ONo** (see Fig. 7, 8 and Table 1), while the J-type stacking of **TPEDKBF₂OEt** and **TPEDKBF₂On** are maintained due to the weaker interactions or the flexibility of the alkyl chains on the left and right sides of the J-type stacking (Fig. 7, 8). Taking **TPEDKBF₂On** as an example, the relatively flexible cavity cannot withstand the applied pressure and collapse before the intermolecular J-type stacking changes under a small amount of isotropic pressure, thus, a smaller blue-shift is observed when **TPEDKBF₂ONo** is smashed. More interesting, **TPEDKBF₂OBu** and **TPEDKBF₂OHe** exhibit sharp blue-shifts but do not have a large pore structure. Although it is difficult to know the specific reason for this, the most notable

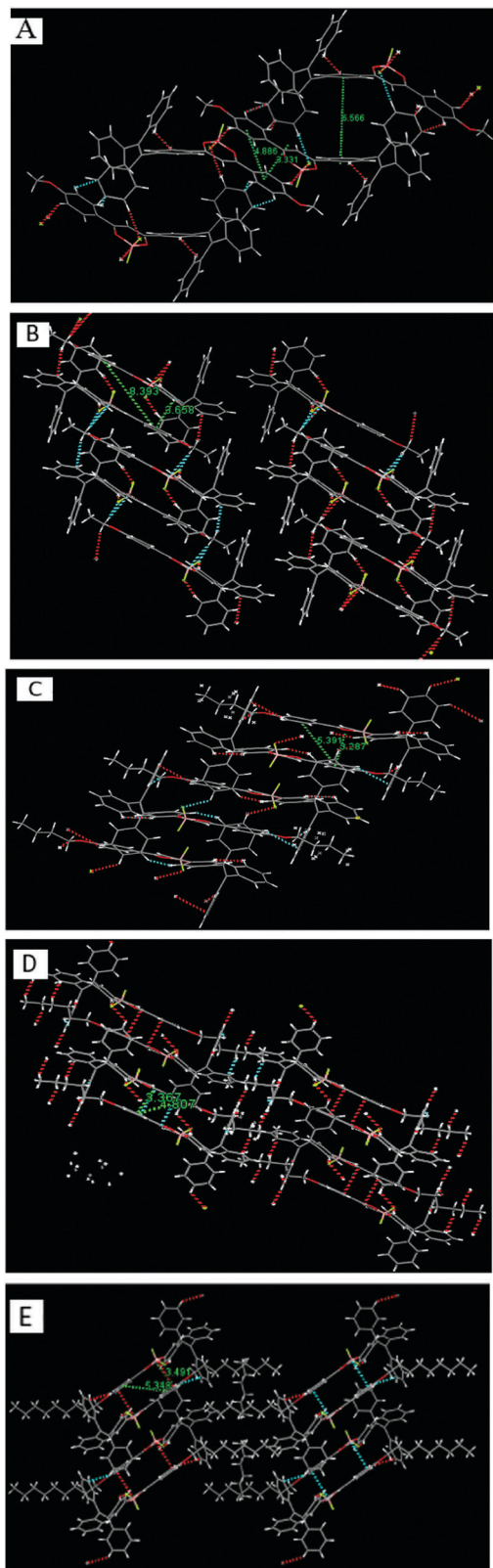


Fig. 8 Molecular stacking mode in the **TPEDKBF₂OMe** (A), **TPEDKBF₂OEt** (B), **TPEDKBF₂OBu** (C), **TPEDKBF₂OHe** (D), **TPEDKBF₂ONo** (E) crystals.

difference is that J-type stacking of **TPEDKBF₂OEt** has a greater overlap compared with that of **TPEDKBF₂OBu** and **TPEDKBF₂OHe**.

Compared to smashing, ultrasonic treatment was found to have a more destructive effect on the intermolecular J-type stacking, and brought about a remarkable blue-shift in the wavelength for all of the synthetic dyes. More interestingly, the long alkyl chain was observed to form a non-polar hydrophobic cavity on both sides of **TPEDKBF₂ONo**, and two hexane solvent molecules adopt an almost orthogonal spatial arrangement with the alkyl chain and form a hydrophobic cavity, but no intermolecular interactions are found between hexane and the **TPEDKBF₂ONo** molecule. The nonpolar environment induced by the long alkyl chain and hexane molecules endows **TPEDKBF₂ONo** with close to the theoretical solid state fluorescence quantum efficiency. Contrary to the effects of ultrasonic treatment and smashing, all of the complexes emit a similar orange fluorescence after grinding. Based on the fluorescence lifetime before/after grinding, the mechanochromic behaviour of the complexes can be attributed to the planarization of the molecular configuration.

Conclusions

A series of organic boron complexes containing a TPE unit and different alkyl chain lengths were designed and synthesized, and based on the investigation of their AIE effect, solid-state fluorescence and mechanochromic properties, the AIE luminogens were found to exhibit excellent solid state fluorescence emission. The highest fluorescence quantum efficiencies were 0.98 and 0.80 in the crystalline and amorphous state, respectively. Although the maximum fluorescence emission wavelength of the crystalline and amorphous state generally adheres to a regular blue-shift upon an increase in the alkyl chain lengths before/after grinding, the maximum wavelength shifts show an irregular wavelength dependence, which mainly depends on the initial fluorescence emission of the crystal. Upon grinding, exposure to ultrasound and being smashed, these complexes display three different colours, among them, a red-shift in the maximum fluorescence emission wavelength was observed due to a phase transition from the crystalline to amorphous state and the planarization of the molecular configuration after grinding, while a blue-shift in the maximum fluorescence emission wavelength was observed due to the destruction of the head-to-head J type stacking after being exposed to ultrasound and being smashed. Compared to being smashed, the blue-shift effect of ultrasonic treatment is more obvious, and the degree of the blue-shift brought about after smashing is closely related to the size and rigidity of the porous structure. Last but not least, a long alkyl chain is advantageous for enhancing the solid-state fluorescence emission and decreasing the phase transition temperature due to hydrophobic interactions and the formation of nonpolar environments.

Conflicts of interest

There are no conflicts to declare.

Acknowledgements

This work was supported by the National Natural Science Foundation of China (Grant No. 21766030, 21566034, 11774255), the key program of the Natural Science Foundation of Tianjin (Grant No. 17JCZDJC30100), and the Seed Program of Tianjin University (Grant No. 2017XZC-0090).

References

- 1 F. Tang, J. Peng, R. Liu, C. Yao, X. Xu and L. Li, *RSC Adv.*, 2015, **5**, 71419–71424.
- 2 G. Yongyang, T. Yejiang, L. Jun, L. Ping, F. Cunfang, Y. Wang Zhang, L. Yawei, S. Jing Zhi, H. Gufeng and Z. Yongming, *Chem. Commun.*, 2013, **49**, 4009–4011.
- 3 S. Zeng, D. Zhang, W. Huang, Z. Wang, S. G. Freire, X. Yu, A. T. Smith, E. Y. Huang, H. Nguon and L. Sun, *Nat. Commun.*, 2016, **7**, 11802.
- 4 Y. Qi, Y. Wang, Y. Yu, Z. Liu, Y. Zhang, Y. Qi and C. Zhou, *J. Mater. Chem. C*, 2016, **4**, 11291–11297.
- 5 Y. Qi, Y. Wang, Y. Yu, Z. Liu, Y. Zhang, G. Du and Y. Qi, *RSC Adv.*, 2016, **6**, 33755–33762.
- 6 F. P. Macedo, C. Gwengo, S. V. Lindeman, M. D. Smith and J. R. Gardinier, *Eur. J. Inorg. Chem.*, 2008, 3200–3211.
- 7 D. R. Yoshii, K. Suenaga, D. K. Tanaka and P. Y. Chujo, *Chem. – Eur. J.*, 2015, **21**, 7231–7237.
- 8 K. Yasuhiro, T. Syunki, F. Kazumasa and M. Masaki, *Org. Lett.*, 2012, **14**, 4682–4685.
- 9 L. Chia-Wei, R. M. Rajeswara and S. Shih-Sheng, *Chem. Commun.*, 2015, **51**, 2656–2659.
- 10 G. Petra, R. C. Korošec, V. Maja and K. Boris, *J. Am. Chem. Soc.*, 2014, **136**, 7383–7394.
- 11 R. Yoshii, A. Nagai, K. Tanaka and Y. Chujo, *Chem. – Eur. J.*, 2013, **19**, 4506–4512.
- 12 Z.-Q. Zhang, Z. Wu, J.-B. Sun, B.-Q. Yao, G.-H. Zhang, P.-C. Xue and R. Lu, *J. Mater. Chem. C*, 2015, **3**, 4921–4932.
- 13 C. Arivazhagan, A. Maity, K. Bakthavachalam, A. Jana, A. Chowdhury, S. K. Panigrahi, E. Suresh, P. S. Mukherjee, A. Das and S. Ghosh, *Chem. – Eur. J.*, 2017, **23**, 7046–7051.
- 14 S. Wang, H.-C. Lan, S.-Z. Xiao, R.-H. Tan and Y.-X. Lu, *Chem. – Asian J.*, 2017, **12**, 198–202.
- 15 P.-Z. Chen, H. Zhang, L.-Y. Niu, Y. Zhang, Y.-Z. Chen, H.-B. Fu and Q.-Z. Yang, *Adv. Funct. Mater.*, 2017, **27**, 1700332.
- 16 P. Galer, R. C. Korosc, M. Vidmar and B. Šket, *J. Am. Chem. Soc.*, 2014, **136**, 7383–7394.
- 17 Z.-Y. Ma, Z.-J. Wang, M.-J. Teng, Z.-J. Xu and X.-R. Jia, *ChemPhysChem*, 2015, **16**, 1811–1828.
- 18 W. A. Morris, M. Kolpaczynska and C. L. Fraser, *J. Phys. Chem. C*, 2016, **120**, 22539–22548.
- 19 Y.-P. Qi, Y.-T. Wang, G.-X. Ge, Z.-Y. Liu, Y.-J. Yu and M. Xue, *J. Mater. Chem. C*, 2017, **5**, 11030–11038.
- 20 A. Kishimura, T. Yamashita, K. Yamaguchi and T. Aida, *Nat. Mater.*, 2005, **4**, 546–549.
- 21 S. Hirata and T. Watanabe, *Adv. Mater.*, 2006, **18**, 2725–2729.
- 22 S.-J. Lim, B.-K. An, S. D. Jung, M.-A. Chung and S. Y. Park, *Angew. Chem., Int. Ed.*, 2004, **43**, 6346–6350.
- 23 C. E. Olson, M. J. R. Previte and J. T. Fourkas, *Nat. Mater.*, 2002, **1**, 225–228.
- 24 M. Irie, T. Fukaminato, T. Sasaki, N. Tamai and T. Kawai, *Nature*, 2002, **420**, 759–760.
- 25 L. Yuan, W. Lin, K. Zheng, L. He and W. Huang, *Chem. Soc. Rev.*, 2013, **42**, 622–661.
- 26 L. Wang, Y. Xiao, W. Tian and L. Deng, *J. Am. Chem. Soc.*, 2013, **135**, 2903–2906.
- 27 W. Piao, S. Tsuda, Y. Tanaka, S. Maeda, F. Liu, S. Takahashi, Y. Kushida, T. Komatsu, T. Ueno, T. Terai, T. Nakazawa, M. Uchiyama, K. Morokuma, T. Nagano and K. Hanaoka, *Angew. Chem., Int. Ed.*, 2013, **52**, 13028–13032.
- 28 Z. Chi, X. Zhang, B. Xu, X. Zhou, C. Ma, Y. Zhang, S. Liu and J. Xu, *Chem. Soc. Rev.*, 2012, **41**, 3878.
- 29 X. Zhang, Z. Chi, Y. Zhang, S. Liu and J. Xu, *J. Mater. Chem. C*, 2013, **1**, 3376.
- 30 Y. Sagara, S. Yamane, M. Mitani, C. Weder and T. Kato, *Adv. Mater.*, 2016, **28**, 1073–1095.
- 31 Y. Zhang, J.-H. Wang, J. Zheng and D. Li, *Chem. Commun.*, 2015, **51**, 6350–6353.
- 32 C. Ma, X. Zhang, Y. Yang, Z. Ma, L. Yang, Y. Wu, H. Liu, X. Jia and Y. Wei, *Dyes Pigm.*, 2016, **129**, 141–148.
- 33 K. C. Naeem, A. Subhakumari, S. Varughese and V. C. Nair, *J. Mater. Chem. C*, 2015, **3**, 10225–10231.
- 34 Y. Cao, Y. Xi, X. Teng, Y. Li, X. Yan and L. Chen, *Dyes Pigm.*, 2017, **137**, 75–83.
- 35 S. Xue, X. Qiu, Q. Sun and W. Yang, *J. Mater. Chem. C*, 2016, **4**, 1568–1578.
- 36 C. Ma, X. Zhang, L. Yang, Y. Li, H. Liu, Y. Yang, G. Xie, Y.-C. Ou and Y. Wei, *Dyes Pigm.*, 2017, **136**, 85–91.
- 37 S. A. Ceballos, S. Gil and A. M. Costero, *RSC Adv.*, 2017, **7**, 14279–14282.
- 38 C. Ma, X. Zhang, Y. Yang, Z. Ma, L. Yang, Y. Wu, H. Liu, X. Jia and Y. Wei, *J. Mater. Chem. C*, 2016, **4**, 4786–4791.
- 39 Q. K. Sun, W. Liu, S. A. Ying, L. L. Wang, S. F. Xue and W. J. Yang, *RSC Adv.*, 2015, **5**, 73046–73050.
- 40 Z. Chen, Y. Nie and S. H. Liu, *RSC Adv.*, 2016, **6**, 73933–73938.
- 41 Y. Liu, Y. Lei, F. Li, J. Chen, M. Liu, X. Huang, W. Gao, H. Wu, J. Ding and Y. Cheng, *J. Mater. Chem. C*, 2016, **4**, 2862–2870.
- 42 Y. Lei, Y. Zhou, L. Qian, Y. Wang, M. Liu, X. Huang, G. Wu, H. Wu, J. Ding and Y. Cheng, *J. Mater. Chem. C*, 2017, **5**, 5183–5192.
- 43 W. Yang, C. Liu, Q. Gao, J. Du, P. Shen, Y. Liu and C. Yang, *Opt. Mater.*, 2017, **66**, 623–629.
- 44 L. Zhou, D. Xu, H. Gao, A. Han, Y. Yang, C. Zhang, X. Liu and F. Zhao, *RSC Adv.*, 2016, **6**, 69560–69568.
- 45 Y. Yue, T. Kurokawa, M. A. Haque, T. Nakajima, T. Nonoyama, X. Li, I. Kajiwara and J. P. Gong, *Nat. Commun.*, 2014, **5**, 4659–4667.
- 46 L. Wang, K. Wang, B. Zou, K. Ye, H. Zhang and Y. Wang, *Adv. Mater.*, 2015, **27**, 2918–2922.
- 47 L. Peng, Y.-N. Chen, Q. D. Yong, C. He and H. Wang, *J. Mater. Chem. C*, 2017, **5**, 557–565.